Experimental Mechanics (2010) 50:1129–1147
DOI 10.1007/s11340-010-9404-9

Recent Applications of Moiré Interferometry

P.G. Ifju · B. Han

Received: 6 July 2010 / Accepted: 17 August 2010 / Published online: 28 September 2010
© Society for Experimental Mechanics 2010

Abstract Moiré interferometry has been a valuable experimental technique for the understanding of the mechanical behavior of materials and structures. Over the last decade less emphasis has been placed on the development of the technique and more towards applications. This paper is a review article on recent applications using moiré interferometry in the fields of microelectronics devices, material characterization, micromechanics, residual stress, composite materials, fracture mechanics, and biomechanics. The general principles of moiré interferometry and advancement of techniques will not be discussed in this text, but references will be provided.

Keywords Moire interferometry · Microelectronics devices · Material characterization · Micromechanics · Residual stress · Composite materials · Fracture mechanics · Biomechanics

Introduction

Moiré interferometry [1] is a well established optical method for the measurement of in-plane displacements on the surface of solids. It utilizes coherent light (typically lasers) to form an interferometer (optical assembly) and a diffraction grating replicated on the surface of the subject. The interferometer directs two pairs of collimated wavefronts, a pair for each orthogonal direction, to the specimen diffraction grating at specific angles. When the specimen and thus grating deform, the diffracted wavefronts interfere to produce fringe patterns that represent the in-plane displacements on the surface of the sample. Subsequent analysis of the two displacement fields using strain displacement relationships provides the strain field. Modern methods of phase-shifting are often employed to automate the fringe analysis procedure and help define the sign of the displacement and strain information. For the most part, the technique is limited to flat surfaces, although provisions for singly curved surfaces have been made. Additionally, the size of the area of interest is typically on the order of 5 cm by 5 cm or smaller. Recent studies using microscopes have made it possible to achieve a viewing area as small as 200 μm×200 μm. The technique has been thoroughly documented in numerous texts and papers that describe the history, theory, implementation, and application. This paper will only cover recent applications (from the late 1990s to the present).

In an article titled "Perspectives in Experimental Solid Mechanics", published in the International Journal of Solids and Structures, in 2000, W. Knause [2] reviewed the significance of experimental methods for the advancement of the understanding of mechanical phenomena in solids. In that article he singled out moiré interferometry as a tool that has both high measurement and spatial resolution. The following quote is taken from that paper. "Perhaps the interferometric and moiré interferometric methods deserve special attention because of their power to resolve displacements measured in terms of the wavelength of light (~ one micron) and because of their potential (when used carefully) for high spatial resolution of the displacement field. These two methods also illustrate the evolution of experimental methods over the last 100 years and thus

This is the 7th in a series of featured review articles to celebrate the 50th anniversary of Experimental Mechanics. These articles serve to touch on both areas of mechanics where the journal has contributed extensively in the past and emergent areas for the future.

P. Ifju (✉, SEM member)
Mechanical and Aerospace Engineering, University of Florida, Gainesville, FL 32611, USA
e-mail: ifju@ufl.edu

B. Han (SEM Fellow)
Mechanical Engineering Department, University of Maryland, College Park, MD 20742, USA

demonstrate how the need in a certain science field (solid mechanics) culls a new method (moiré interferometry) from a well established physical principle for a special application." He goes on to say, "Because of this high resolution power of moiré interferometry, it has been an important addition to the repertoire of tools for experiments and became thus a favorite tool for refined deformation measurements on electronic micro chips; in this connection this method has served virtually the same purpose for these small devices as photoelasticity has for the larger engineering structures during the middle of this century; the major difference being that photoelasticity addresses the stress state more directly than moiré interferometry, which renders displacements."

This statement summarizes the state of moiré interferometry contributions at the beginning of the last decade. Since then, moiré has continued to be an invaluable tool in our quest to understand mechanical phenomena.

The theory of the moiré interferometry technique can be found in numerous publications including those written by groups led by Post [1, 3–5], Mckelvie [6–9], Walker [10–12], Cloud [13], Dai [14–17], Morimoto [18, 19] and the current contributing authors. In this text we will expand on recent applications in the research on microelectronics devices, material characterization, micromechanics, residual stress, composite materials, fracture mechanics, and biomechanics. In the short format associated with Experimental Mechanics it is impossible to cover all applications. The ones covered represent only a fraction and the authors apologize for those omitted in this text.

Microelectronics Device

Microelectronics devices contain many electronic components within an active silicon chip, such as transistors, capacitors, resistors, etc. To form a usable device, a silicon chip requires protection from the environment as well as both electrical and mechanical connections to the surrounding components. The various conducting and insulating materials involved in the devices have different coefficients of thermal expansion (CTE). When the chip is powered up and thus the device is subjected to a temperature excursion, each material expands at a different rate. This non-uniform CTE distribution produces thermally induced mechanical stresses within the device assembly. As the components and structures involved in high-end microelectronics devices are made smaller, the thermal gradient increases and the strain concentrations become more serious. Hence, there is a continuously increasing activity in experimental analysis, both for specific studies and for guidance of numerical analyses. Moiré interferometry has been taking a leadership role for experimental analyses since Guo and his co-workers introduced a special technique to apply gratings on specimens with a complex geometry [20].

A special technique is required for the cross sections of microelectronics devices because they usually have such a complex geometry that the excess epoxy produced by the usual grating replication procedure cannot be removed [20, 21]. The excess epoxy is critical since it could reinforce the specimen and change the local strain distribution. An effective replication technique was developed to circumvent the problem. First, a tiny amount of liquid epoxy is dropped onto the grating mold; the viscosity of the epoxy should be extremely low at the replication temperature. Then, a lintless optical tissue (a lens tissue) is dragged over the surface of the mold, as illustrated in Fig. 1. The tissue spreads the epoxy to produce a very thin layer of epoxy on the mold. The specimen is pressed gently into the epoxy, and it is pried off after the epoxy has polymerized. Before polymerization, the surface tension of the epoxy pulls the excess epoxy away from the edges of the specimen. The result is a specimen grating with a very clean edge.

The early applications of moire interferometry used a bithermal loading [22]. In this technique, the specimen grating is applied at an elevated temperature, and then the specimen is allowed to cool to room temperature before it is observed in the moiré interferometer. Thus, the deformation incurred by the temperature increment is locked into the grating and recorded at room temperature. Numerous examples can be found in the literature [20, 21, 23–41].

An example is illustrated in Fig. 2 [24, 35, 41]. The specimen is a flip-chip plastic ball grid array (FC-PBGA) package assembly. In the assembly, a silicon chip (6.8 mm× 6.1 mm×1.2 mm) was first attached to an organic substrate through tiny solder bumps called C4 interconnections. The gap between the chip and the substrate was filled with an epoxy underfill to reduce the strains of solder bumps. This subassembly was then surface-mounted to a typical FR-4 printed circuit board (PCB) through larger solder ball arrays to form a final assembly. The assembly was cut and its cross-section was ground to produce a flat, smooth, cross-sectional surface. The specimen grating was replicated at 82°C and the fringes were recorded at room temperature (ΔT=−60°C).

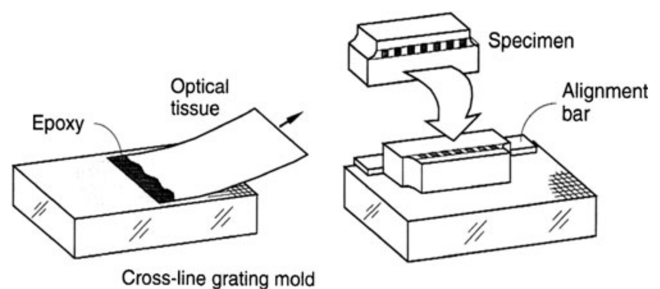

Fig. 1 Replication procedure for small specimens of complex geometry

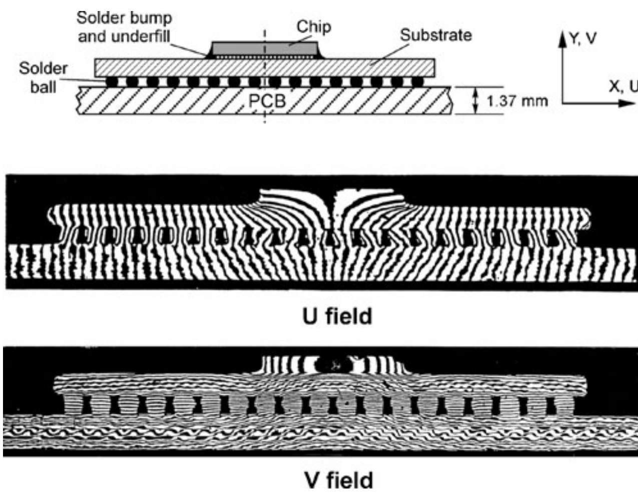

Fig. 2 *U* and *V* displacement fields of FC-PBGA package assembly, induced by a bi-thermal loading of ΔT=−60°C

Very clean edges of the specimen grating are evident. The substrate had a higher coefficient of thermal expansion (CTE) than the PCB. The substrate contracted more than the PCB during cooling, while the deformation of the substrate covered by the chip was constrained by the low CTE of the chip. This complicated loading condition produced an uneven curvature of the substrate. The substrate was connected to the PCB through the solder balls and the difference of curvature between the substrate and the PCB was accommodated by the deformation of the solder balls. The experimental evidence provided by moiré interferometry was essential to revealing important design parameters.

The bi-thermal loading was extended to cyclic loadings, where the package assemblies were subjected to thermal cycles or mechanical cycles first and residual deformations were documented at room temperature. Han [27] determined inelastic damage accumulations in solder columns of a ceramic column grid array assembly after subjecting it to thermal cycles. Later, Basaran et al. [42], Liu et al. [43] and Tunga and Sitararman [44] used a similar procedure for BGA assemblies but at the much higher number of cycles, and Kwon et al. [45] for an assembly using anisotropic conductive adhesive. Zhao and Basaran also measured the inelastic deformations of solder joints, caused by vibrations and shocks [46].

Thermal-cycling induced residual deformations documented by moire interferometry are illustrated in Fig. 3 [27]. The specimen was a ceramic column grid package assembly [Fig. 3(a)] which was subjected to four thermal cycles of 125°C and −40°C. The residual U and V displacement fields of the column are shown in (b), which were used to determine the deformed shape of the column (c). After

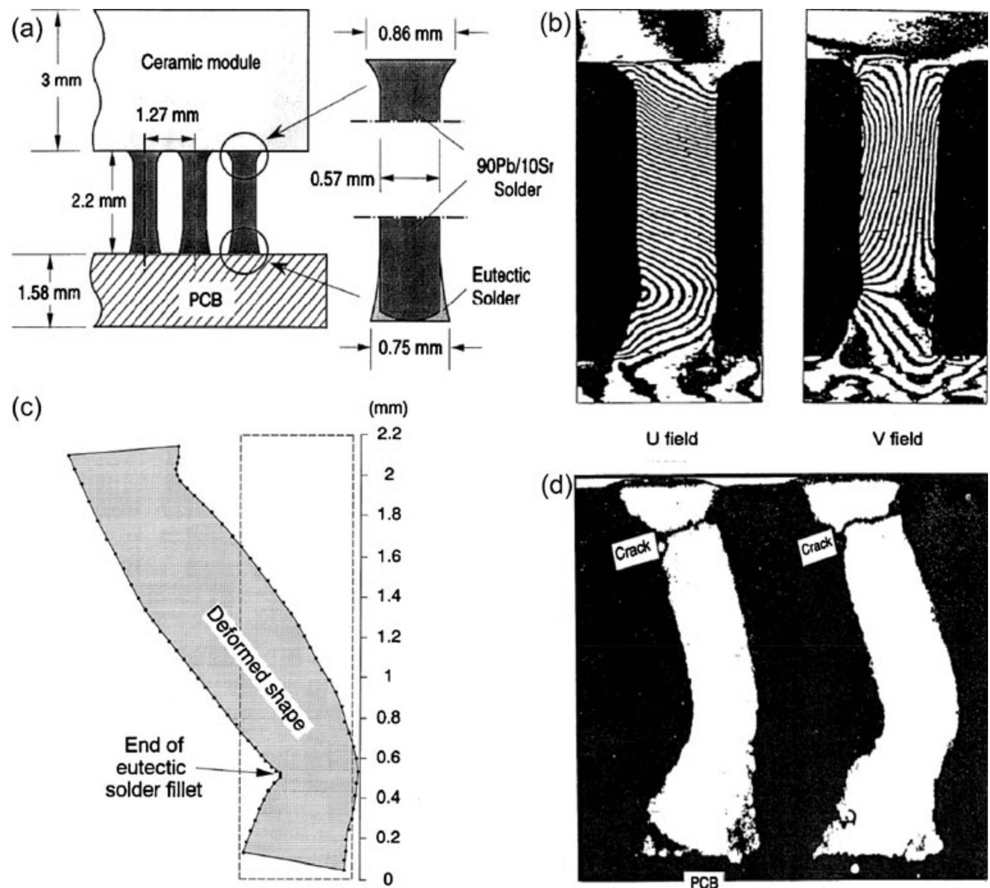

Fig. 3 Column grid package (**a**) assembly; (**b**) U and V displacements and (**c**) exaggerated deformed shape of solder column after four thermal cycles, and (**d**) failed column after the actual ATC test

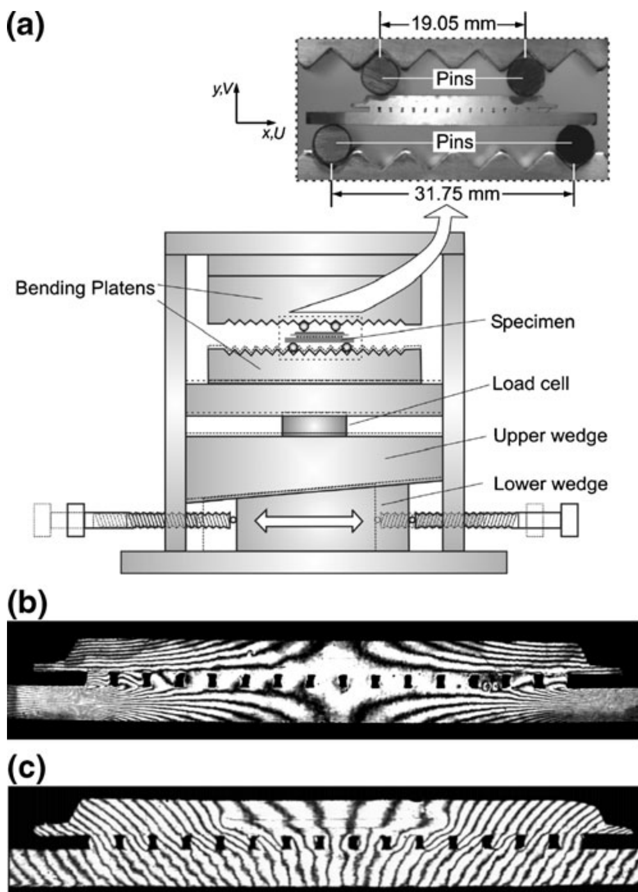

Fig. 4 (**a**) Schematic diagram of a flexure test apparatus (the insert shows the positions of specimen and loading pins). Representative U field fringe patterns produced (**b**) by mechanical bending of 28.2 N·mm and (**c**) by thermal loading by heating to 80°C (Courtesy of J. Joo, Chungbuk National University)

thermal cycles, the column surrounded by the eutectic solder fillet experienced much more severe permanent deformation, which increased the bending deformation at the top. This effect was confirmed by the results from an actual accelerated thermal cycling (ATC) test.

The applications were further extended into the domain of real-time observation under a mechanical loading [47–49]. Stout et al. measured deformations of the PBGA assembly subjected to four-point bending [47]. Later Wang et al. [48] used four-point bending to investigate the effect of packaging on the Cu/Low-k interconnects, and Joo et al. [49] also used four-point bending to investigate different deformation modes caused by the mechanical bending while comparing them with the thermo-mechanical deformation modes. Figure 4(a) shows schematically a flexure test apparatus (the insert shows the positions of specimen and loading pins) used in [49]. The mechanical loading induced deformation (b) shows a symmetric deformation causing the maximum deformation in the outmost solder ball, while the thermally-induced deformation (c) caused the maximum deformation at the solder ball directly under the edge of the chip.

More recently, robust schemes of moire interferometry became available for real-time observations of thermally-induced deformations, most notably PEMI (Portable Engineering Moiré Interferometer). They were employed to study the temperature-dependent thermo-mechanical behavior. The schemes were implemented with convection-type or conduction-type environmental chambers that provide the temperature control required in accelerated thermal cycling (isothermal loading) [35, 41, 50–65]. Park et al. [66] and Yang et al. [67] tested package assemblies under power cycling by heating the chip directly. Figure 5 shows the schematic of the experimental setup of the power cycling and U field moiré fringes obtained during the cycling [66].

Other loading conditions were also used to measure deformations. Ye et al. [68, 69] measured the *in situ* displacement evolution of lead-free solder joints under electric current stressing. Stellrecht et al. [70, 71] developed an effective scheme to measure deformations induced only by hygroscopic swelling. Later Tsai et al. [72] and Park et al. [73] used a similar procedure to measure hygroscopic deformations of a plastic package and a conductive adhesive

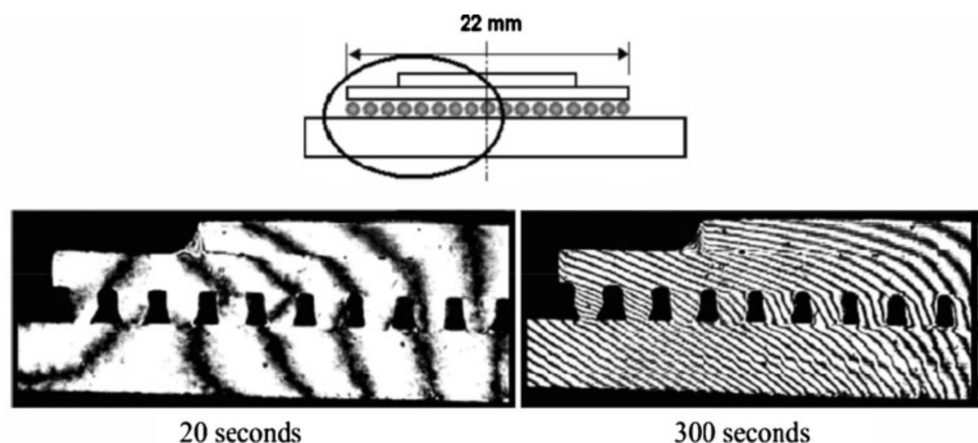

Fig. 5 Schematic of the experimental setup of power cycling and U field moire fringes at two different times (Courtesy of S. B. Park, SUNY Binghamton)

package, respectively. Figure 6 illustrates the deformation induced by hygroscopic swelling, where fringe patterns were obtained at 85°C after subjecting a plastic package to 85°C/85%RH [71].

Material Characterization

Traditionally, material property characterization is performed using standard test methods and conventional strain measurement techniques such as strain gages and extensometers. With the ever increasing complexity of material behavior, comes the need for more advanced methods for characterizing then. For instance active materials, or smart materials, undergo phase changes that can be complicated by hysteresis, and thermal effects. Full-field methods can provide valuable information that can be used to understand the physics of how such materials behave and thus help to build and validate numerical models.

Perry et al. [74] used moiré interferometry to study the deformation in SE-508 seamless drawn tubing heat treated at 500 C. Figure 7 shows a sequence of wrapped fringe patterns during the tensile loading of the material at a temperature above the austenite finishing temperature. Transformation to martensite initiates at the top and bottom of the gage section and works its way towards the center of the specimen. From this test the stress versus strain behavior from both a global measurement and the local measurement, taken from the moiré fringe patterns could be extracted from the sample.

The documentation of material heterogeneity is enhanced by the use of full-field methods. Guo et al. [75] recently reported deformation of polycrystalline aluminum alloys using moiré interferometry. They studied a specimen whose grain size was on the same scale as the width of the tensile specimen that was used for loading. They were able to

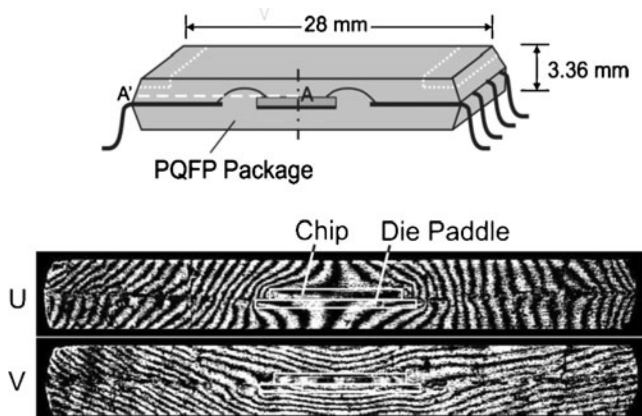

Fig. 6 Fringe patterns obtained at 85°C after complete moisture absorption (Courtesy of E. Stellrecht, Sierra Research)

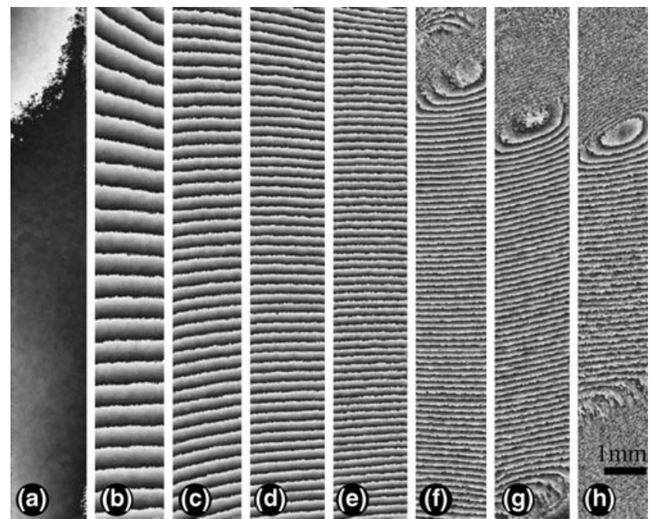

Fig. 7 The vertical displacement field for a Nitinol tensile specimen undergoing phase transformation (Courtesy of Perry)

extract the strains from individual grains and build a global and local stress-strain response. Figure 8 shows the region of the specimen that was studied, and the horizontal and vertical displacement fields. The grain boundaries are visible and the heterogeneous behavior can be seen in the fringe patterns.

For simple tensile tests on isotropic materials, the stress-strain curve and Poisson's ratio can be extracted using conventional strain measurement approaches. These two constants are the only ones needed to characterize the linear stress-strain behavior. For anisotropic materials, there are more constants, and as such, more tests are required to extract the constants thus adding time and expense to the process of characterization. As a result, there has been a push to employ a single specimen of complex geometry, full-field measurements, and inverse methods to determine multiple material properties in orthotropic materials. In 2004 Wang et al. [76] used moiré interferometry in combination with a circular disk, loaded in diametrical compression, to extract material properties from an isotropic material to demonstrate the potential of the inverse method approach. Figure 9 shows the loading condition, the theoretical displacement field (horizontal field in this case), a wrapped moiré displacement field and an unwrapped displacement field. They used least squares to evaluate the differences in the model and experiment. It was shown that the method could determine the modulus of elasticity and the Poisson ratio to within 3% of the handbook value.

An open-hole tension specimen was employed by Molimard et al. [77] to measure four orthotropic plate constants from a single geometry. They used phase-shifted moiré interferometry to measure full-field surface displacement and strain. Figure 10 shows the geometry and loading fixtures used in their tests. Displacement and strain contours were measured in the area around the open-hole.

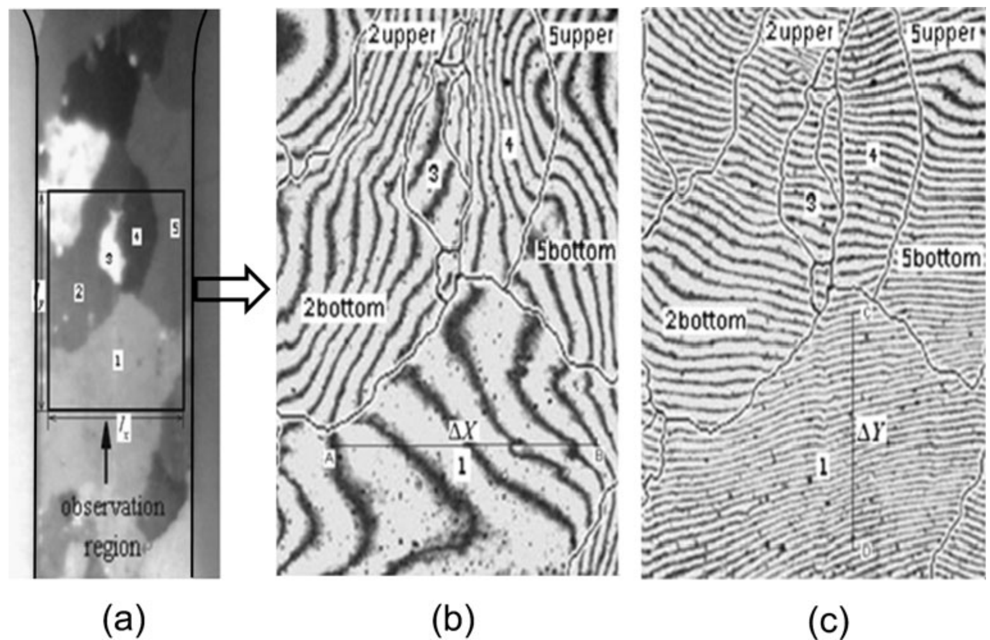

Fig. 8 The deformation heterogeneity can be seen in the moiré interferometry fringe patterns applied to polycrystalline aluminum alloy (Courtesy of Guo)

The principal employed was to minimize the discrepancy between experimental and theoretical strain results using a Levenberg-Marquardt algorithm. Comparisons between the experimental and analytical shearing strain values are presented in Fig. 10. The method takes into consideration the optical system, signal processing, and the mechanical aspects. Cost functions were investigated leading to a simple mathematical form. Two models were used: an analytical model based on the Lekhnitskii approach and the finite element method. The researchers were able to identify the four elastic constants to within 6% of those measured using traditional means.

Aside from mechanical properties such as modulus of elasticity and Poisson's ratio, there are other material properties that are of interest to engineers. When utilizing concrete, for instance, the shrinkage during cure as a function of composition, time, humidity, and temperature plays a vital role in the ultimate strength and integrity (free from cracks). There have been numerous methods developed to understand this complex phenomena. Recently, Chen et al. used moiré interferometry and inverse methods to determine shrinkage coefficients in cement, mortar and

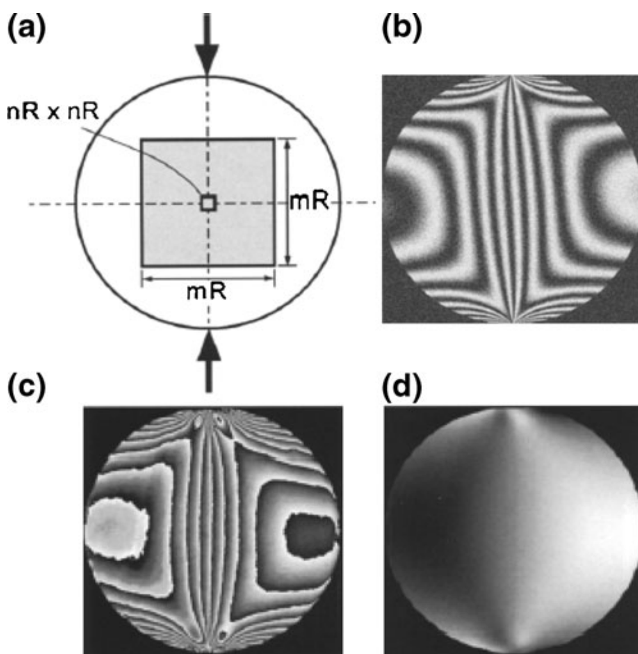

Fig. 9 (**a**) Circular disk in diametrical compression, (**b**) numerical model of horizontal displacements with added noise, (**c**) wrapped moiré interferometry fringe pattern and (**d**) unwrapped horizontal displacement pattern (Courtesy of Z. Wang, Catholic University)

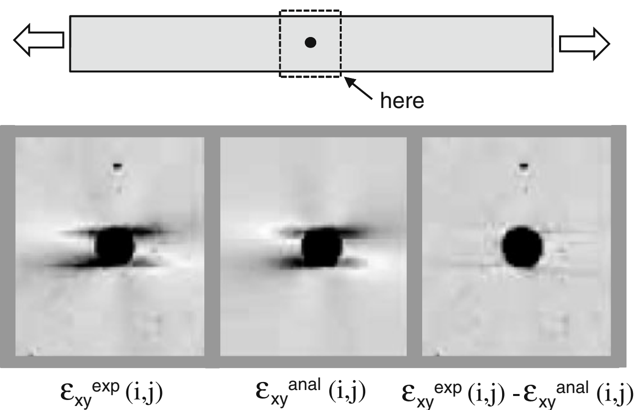

Fig. 10 Open Hole specimen and loading configuration with experimental shear strain distribution, analytic shear strain distribution, and differences after the application of difference minimization using the Levenberg-Marquardt algorithm (Courtesy of Molimard)

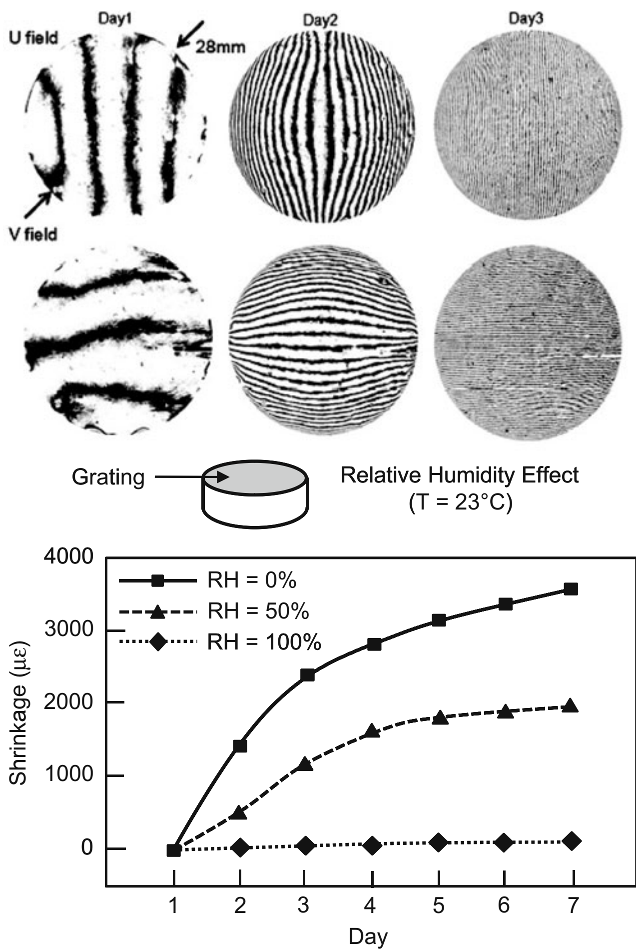

Fig. 11 The average shrinkage across the width of a cement specimen versus time (days) for various combinations humidities. The fringe patterns show the U and V displacement fields for the first 3 days (Courtesy of Chen)

concrete materials [78]. In Fig. 11 the shrinkage of cement can be seen as a function of time at various humidities. The technique utilizes the methodology of the cure reference method, formerly developed for composite residual stresses by attaching a diffraction grating on the cement sample during the initial solidification of the cement. The grating then acts as a datum from which subsequent deformations were measured over a period of 7 days. The method was employed in parallel with an axi-symmetric FEM model that modeled the grating as a semi-permeable membrane.

Micromechanics

Many fields of study require deformation measurements of tiny specimens or tiny regions of larger specimens. The mechanics of microelectronic assemblies is an example, where the ever-increasing demand for closer packing exacerbates the problems of thermal stresses. Other fields include crack-tip analyses in fracture mechanics; grain and intragranular deformations of metals and ceramics; fiber/matrix interactions in fiber reinforced composites; interface problems; etc.

The small size and the need for high spatial resolution require microscopic viewing of the specimen. Microscopic moiré refers to this special implementation of moire interferometry for microscopic viewing [79, 80]. Tiny interferometers were fabricated to accommodate microscope objectives as an imaging system for large deformations (Shield and Kim [79]) and small deformations (Han and Post [80]).

In the approach proposed by Han and Post, an "*immersion interferometer*" was developed, whereby the specimen is coupled optically to the interferometer by a thin layer of immersion fluid to reduce the wavelength of the light propagating in the medium (Fig. 12) and thus increased the upper sensitivity limit of moire interferometry. Later Liou and Prakash [81] proposed a microscopic moiré approach using a transmission diffraction grating that allows a simple and quick change of the virtual reference grating vector without disturbing the optical alignment of the other components in the optical train.

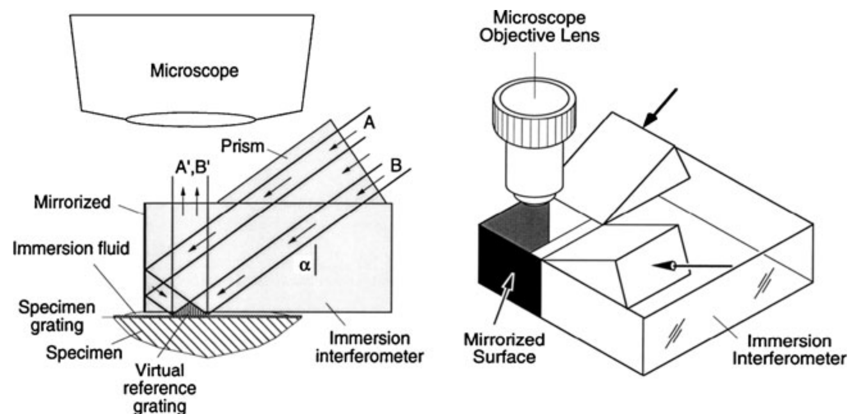

Fig. 12 Optical paths in an immersion interferometer and arrangement for U and V fields in microscopic moiré interferometry

Within a small field of view, the relative displacements are typically small unless the strains are extremely large. For those applications, displacement resolutions were increased by digital image processing techniques: the optical/digital fringe multiplication (O/DFM) method [80, 82] and the phase shifting technique [83].

Bastawros and Kim [84] utilized the approach proposed by Shield and Kim to measure the in-plane components of the Almansi strain tensor. La Porta et al. [83] used microscopic moiré interferometry with the phase shifting technique to investigate the near-tip fields of a precracked stainless steel specimen under load. The approach proposed by Han and Post was combined with the O/DFM method to document the heterogeneous deformation of titanium in elastic tension [85], the fiber/matrix interactions in a unidirectional Boron/Aluminum metal-matrix composite [86], micromechanical thermal deformations of semiconductor packages and subassemblies [30, 41] and the changes in microstrain across bonded dentin interfaces [87]. Figure 13 shows the microscopic displacement fields around two plated-through-holes (PTH), induced by ΔT of −80°C, where the contour interval is 104 nm/fringe [86]. The fringe patterns clearly show the homogenous nature of the plug material inside the PTH and the heterogeneous nature of fiber/resin laminated areas located between the PTHs.

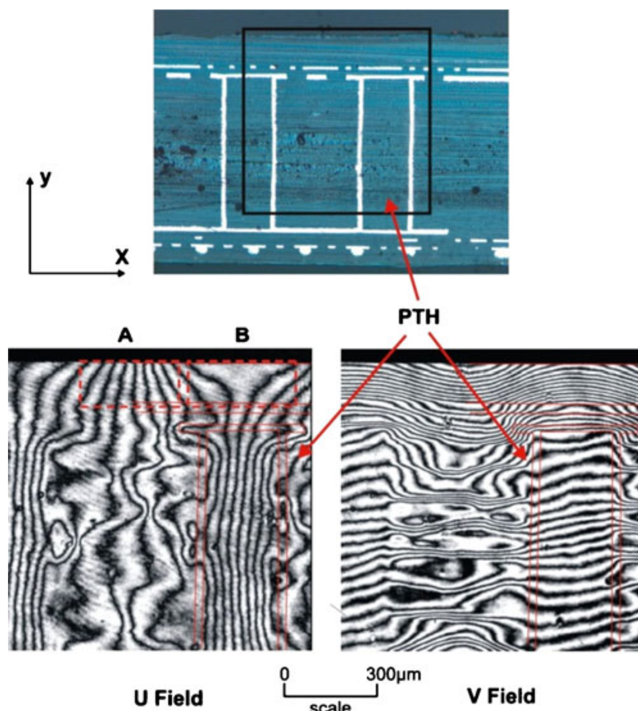

Fig. 13 Local CTE variations around plated-through-hole, induced by ΔT of −80°C. The contour interval is 104 nm/fringe (Courtesy of S. Cho, Intel)

Residual Stress Measurements

In recent years moiré interferometry has been an ever-increasing choice for the investigation of residual stresses in a wide variety of materials, including both homogeneous, isotropic materials and heterogeneous, anisotropic materials, such as fiber reinforced composites. Residual stresses in isotropic materials are induced by non-uniform cooling upon solidification, gradients in material properties, stress history and shot-peening. These stresses can be deleterious to the ultimate load caring capacity of a structure or can be used to suppress tensile stresses and thus they can be advantageous. In composites, residual stresses are produced by the difference in the coefficient of thermal expansion of the constituents (matrix and reinforcement) and the chemical shrinkage of the matrix material during polymerization. In most cases these stresses detract from the ultimate load capacity of the material.

Aside from the full-field nature, high spatial and measurement resolution of moiré interferometry there are other characteristics that make the technique well suited for residual stress measurements. The process of applying the grating to the specimen acts to establish a datum from which subsequent deformation can be referenced. By retaining the grating mold this reference can be recovered through the process of tuning the interferometer to match the grating mold. Subsequent deformations of the specimen grating caused by tractions, temperature change, moisture absorption, chemical shrinkage and machining to release internal stresses can be referenced back to the original undeformed grating. This characteristic has been exploited for hole-drilling, sectioning and composite cure process documentation.

Hole-drilling

The hole-drilling method was originally developed for anisotropic materials by Mathar [88] in 1934. The method relieves stresses via the creation of a free surface (hole surface) and produces a stress/strain gradient in the surrounding material. Strains are traditionally measured with special strain gages [89, 90]. This can be limiting because the strain gradients are not captured by the gage since it only provides average strain values over the area of the gage. As a result, many researchers have utilized full-field methods such as brittle coatings [91], photoelastic coatings [92], holographic interferometry [93], electronic speckle pattern interferometry [13], shearography [94], interferometric strain gages [95] and digital image correlation [96]. In 2010 Schajer [97] wrote a review article on advances in hole-drilling while independently Nelson [98] wrote a review on the determination of residual stresses using optical methods. Both of these, quite recent articles

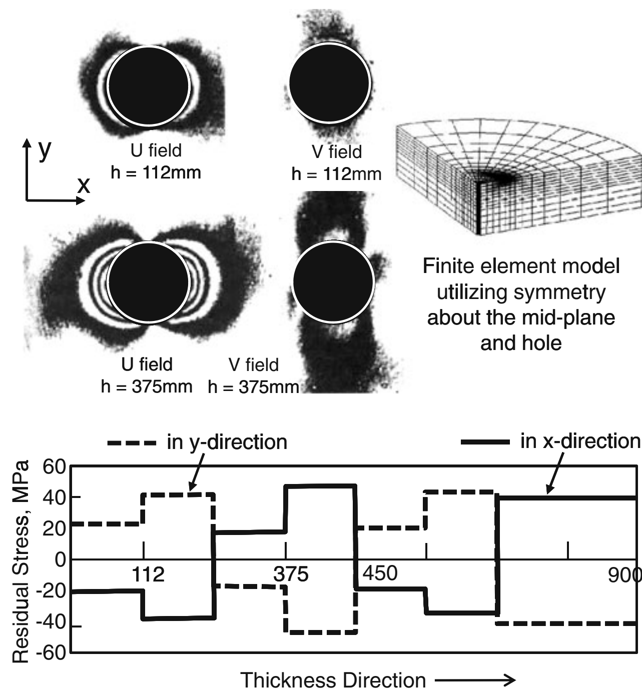

Fig. 14 Moiré fringe patterns for two drill depths, the finite element model used for calibrating coefficients, and the residual stresses as a function of thickness (Courtesy of Wu)

list moiré interferometry as a viable technique that provides good spatial and measurement resolution, can determine the displacements at the hole edge, but can be cumbersome because of grating transfer.

Moiré interferometry was first used for hole-drilling by Nicoletto in 1988 and reported in 1991 [99]. He was able to measure the residual stress in areas dominated by a gradient. Recently, others have utilized the moiré/hole-drilling method for a variety of materials [100–107]. Advances in the technique include the use of automated fringe analysis through the use of fringe shifting, and incremental hole-drilling in combination with moiré. Jian Lu's research group at the University of Technology in Troyes France (UTT) regularly collaborated with numerous practitioners of moiré including F.L. Dai and both of the contributing authors to extend the method of hole-drilling moiré interferometry to new levels. With Han's input the incremental hole-drilling method was established and applied to isotropic materials. In a two part paper, Wu, Lu and Han [104, 105] describe the process and the theoretical analysis methods to determine the stresses from the strain information. Wu et al. [106] then extended the method to measure residual stresses on the ply level of composites. Using a 2 mm diameter drill bit and computer controlled drilling increments coincident with the interfaces between plies, displacement fields were recorded through the thickness of the composite. An expression describing the relationship between displacements on the surface, stresses in each layer, in-plane direction cosines, and a set of coefficients was employed. A rigorous calibration of the constants was performed using the full-field, moiré displacement fields and a 3-D finite element model of the 16 ply composite. Figure 14 shows two sets of moiré displacement patterns around the hole after the mill had drilled to two depths (h in the figure). The investigators were able to determine the residual stresses in each ply of a $[0_2/90_2]_{2s}$ laminate.

In order to automate fringe analysis, phase shifting algorithms have been employed with the hole-drilling method. An example of this can be seen in the study conducted by Ya et al. [101]. Figure 15 shows the resulting wrapped and unwrapped phase distributions extracted from the fringe patterns for a study conducted on shot-peened aluminum.

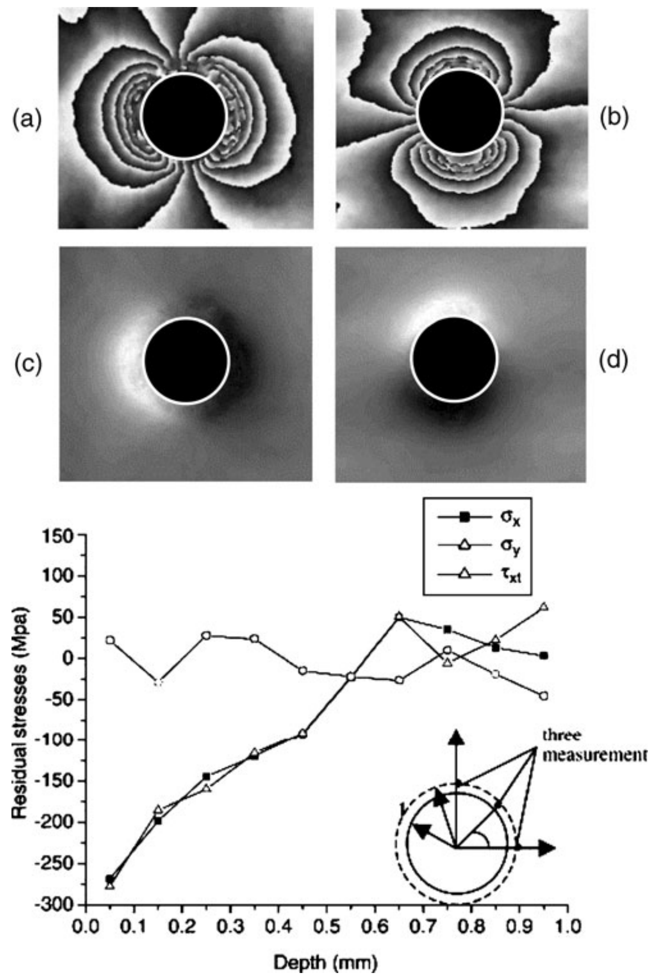

Fig. 15 Wrapped phase distributions for the (**a**) U field (**b**) V field and phase unwrapped distributions for the (**c**) U field and (**d**) V field. Residual stresses as a function of depth are presented for a shot-peened aluminum specimen (Courtesy of Ya)

Composite Sectioning

Much like the hole-drilling method, by sectioning rather than drilling, a free surface is created thus leading to stress/strain redistribution. Whenever a multidirectional laminate is cut, a free edge is created and residual stresses are liberated. Stresses at the free edge must satisfy equilibrium and thus the normal stress perpendicular to, and the shear stress components parallel to the newly developed surface must be zero. Stresses still exist in the interior of the composite, and thus there is a gradient established by forming the free edge. One can measure the strain relief as a result of the creation of the free edge and then relate this to the stresses that existed in the laminate before the cut. There is an underlying assumption that the cutting method itself does not create a deformation field (i.e., no plastic deformation). For most fiber reinforced polymer materials, a well lubricated, slow speed, diamond impregnated cut off wheel has been shown to produce negligible local deformation. This can be verified by cutting a unidirectional composite, where ply level residual stresses do not exist.

A number of researchers have utilized this method to determine the residual stress in laminates [108–112]. Some notable work on the topic was performed by Joh, Gascoigne, Lee and Czarnek. Recently Schoeppner et al. [112] investigated the residual stresses and strain in a composite bonded joint. The study was aimed at validating a polynomial spline displacement approximation method using a thermomechanical linearly elastic analysis. Laminated specimens were bonded together at an elevated temperature and then a diffraction grating was applied to the edge of the composite at room temperature. A cut was then made to liberate stresses. Moiré interferometry was then used to acquire the displacement fields. Fringe shifting was used to determine strain fields and these were compared to the model. Results can be seen in Fig. 16.

Cure Reference Method

The cure reference method [113, 114] introduced in 1999 utilizes moiré interferometry and the application of a diffraction grating on the surface of a composite during the autoclave curing process, as shown in Fig. 17. This grating forms a datum from which subsequent thermal stresses can be referenced. Additionally, the method is capable of measuring the combination of the thermally induced and chemically induced components of strain. Unlike many of the former methods, it is capable of determining the residual stresses on any laminate stacking sequence (not just cross-plies), although standard Kirchoff assumptions are made in the analysis (therefore variations due to through-thickness cure gradients cannot be measured). If the specimen is brought to the cure temperature and the strain is monitored, the thermal and chemical contributions can be separated. By applying the cure reference method to a unidirectional material, the “free residual strain”, defined by the thermal expansion and chemical shrinkage terms combined, can be measured. Then, by applying the cure reference method to a laminate (in the same autoclave cycle) the stresses can be calculated on the ply-scale from the laminate strain information and the free residual strains, within the context of laminate theory.

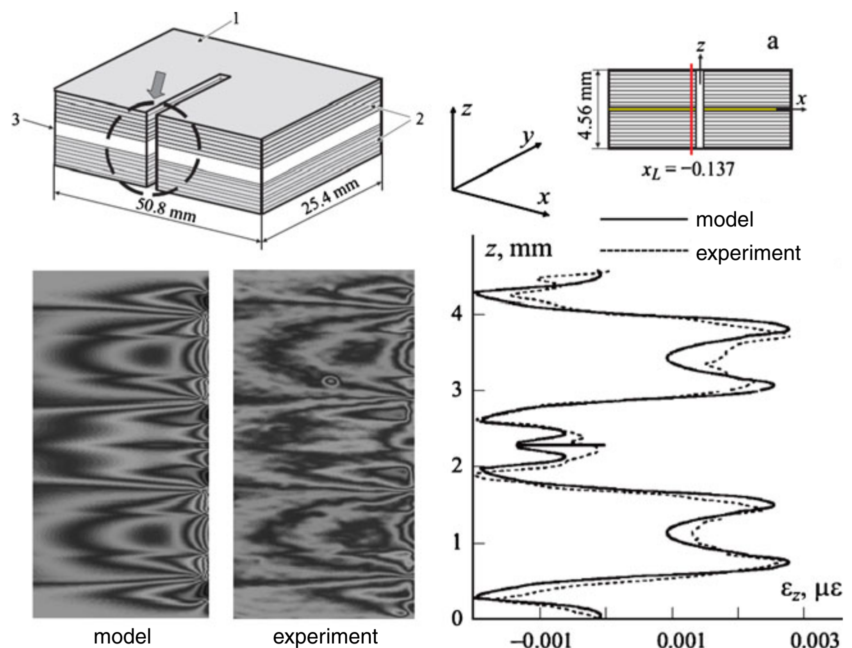

Fig. 16 The vertical strains ε_z, from the numerical model and moiré interferometry, on the surface of a bonded joint are compared (Courtesy of Schoeppner)

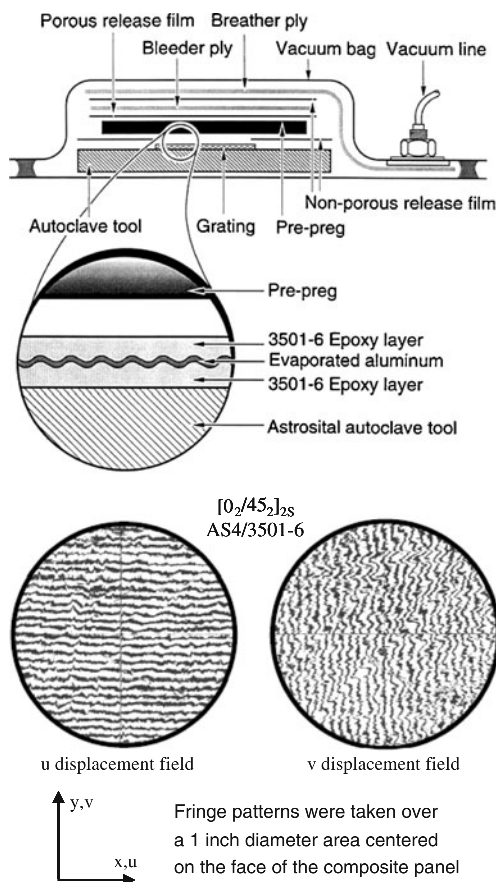

Fig. 17 The cure reference method and fringe patterns of displacement on the surface of a laminated composite

Experiments on the X-33 reusable launch vehicle laminate were conducted at the University of Florida using a combination of the cure reference method and strain gages. The strain on the surface of multidirectional and unidirectional composites was measured through the temperature range from cure to liquid Nitrogen. It was determined that approximately 20% of the strain at cryogenic temperatures originates from chemical shrinkage and the remainder from a thermal expansion mismatch. A series of experiments was performed to determine the dependence of the coefficient of thermal expansion α_2, the modulus E_2 and the shear modulus G_{12} on temperature (these three properties are highly dependent on temperature while the others are nearly independent of temperature). These temperature dependent material properties were then utilized in the analysis. It was shown that the laminate configuration that was presumed to be within a safe operating condition at cryogenic temperature, with a predicted factor of safety of 1.3, actually had a safety factor of 0.8, once the temperature dependent properties and chemical shrinkage residual stresses were incorporated in the analysis. Unfortunately, this analysis was performed after the failure of the fuel tank and the cancellation of the entire X-33 program. In a parallel optimization study, an alternative laminate sequence was developed in order to carry the applied loads, and at the same time, resist residual stress failure. The resulting angle-ply laminate, $[\pm 25]_n$ was tested using the cure reference method in parallel to the X-33 laminate. It was found that it retained a safety factor of 1.8 even when the chemical shrinkage term and the temperature dependent material properties were used in the analysis.

Composite Materials

Through the 1980's and 1990's composite applications represented a large portion of the studies that utilized moiré interferometry. Composites pose a significant challenge because they are heterogeneous on the fiber-scale, ply-scale and in some cases have complex textile architectures that dominate the strain field; therefore high spatial resolution is required to understand their mechanics. Additionally, most of the high performance material systems, such as carbon fiber/epoxy matrix, are quite stiff and the strain range is typically below 1% requiring a technique with high measurement resolution. Moiré interferometry is well suited to make measurements on the ply-scale and through the entire strain range of most composites; therefore it continues to be a valuable experimental technique for composites applications. In this section we will review a number of recent applications that highlight the capabilities of the technique.

Textile Composites

Textile composites utilize reinforcement in the form of a fabric that can be woven, braided, knit or stitched and then combined with matrix materials, via resin transfer techniques, hand lay-up, or prepreg methods. Textiles can have distinct advantages over traditional laminates made from unidirectional layers, including better conformability over complex 3-D tools, enhanced interlaminar strength, cost savings through near net shape production, and better damage tolerance. However, there are potential disadvantages including lower fiber volume fraction, the existence of resin rich volumes between yarns and degraded in-plane properties (as a result of the non-straight path that the yarns, must accommodate). In many cases the advantages outweigh the disadvantages, and as such, they are extensively used in applications from the sporting goods industry to advanced aerospace vehicles.

Textile composites can pose additional challenges to the experimentalist since they have an additional level of heterogeneity. Not only is there heterogeneity on the fiber-scale, but also on the scale of the textile architecture and the

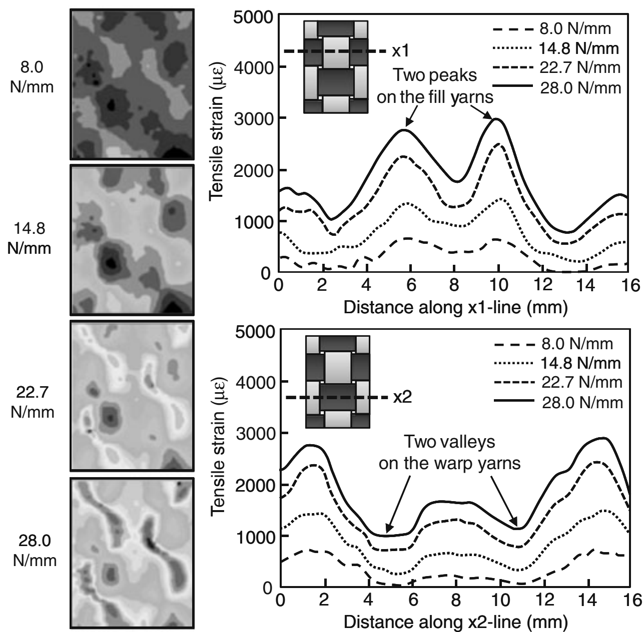

Fig. 18 Tensile strain contour maps for four load levels. Plots along two lines show the variation of strain and correspondence to the textile architecture (Courtesy of J. Lee)

laminate scale (if multiple layers of cloth are used). For many textile forms a yarn may contain 1,000 to 12,000 fibers (or even more), and the repeating unit in the textile architecture may have linear dimensions on the order of 1 cm or more. This can pose significant challenges to the experimentalist, even for seemingly routine tests to determine the elastic properties [115, 116] using strain gages.

It has been assumed that the textile architecture induces repeating spatial variation of strain on the surface coincident with the architecture itself. In order to document the strain distribution associated with the architecture, high spatial and measurement resolution are required. Recent studies using moiré interferometry, have documented the strain field on the surface of composites. These results can be used to guide instrumentation practices for strain gages as well as validate modeling efforts.

Lee et al. [117] used digital phase-shifting grating shearography (essentially moiré interferometry) to experimentally characterize plain-weave, carbon/epoxy composites under tensile loading conditions. They found that the strain varied cyclically and followed the weave architecture. Figure 18 shows contour plots as well as line plots (at two different locations with respect to the architecture) of the tensile strain for four different load levels. The maximum strains were on the order of three times greater than the minimum strain values. In the transverse direction they found that the normal strain is predominantly compressive (Poisson effect), but locally there are regions of tensile strain. These effects are attributed to yarn crimp and bending as a function of axial load.

Shrotriya et al. [118] used moiré interferometry to measure the local time-temperature-dependent deformation of a woven composite used for multilayer circuit boards. They studied both the deformation fields in the plane as well as over the cross-section through a temperature range of 27°C to 70°C. The measurement over the cross-section demonstrates the spatial resolution of the method. Their measurements revealed the influence of the fabric architecture in the deformation field. They noted that the variation in strain was greater when the composite was loaded in the fill direction (versus the warp direction) due to higher crimp angles (the angle that defines the undulation of a yarn as is passes over and under the transverse yarn). They also found that the total deformation increased with temperature and

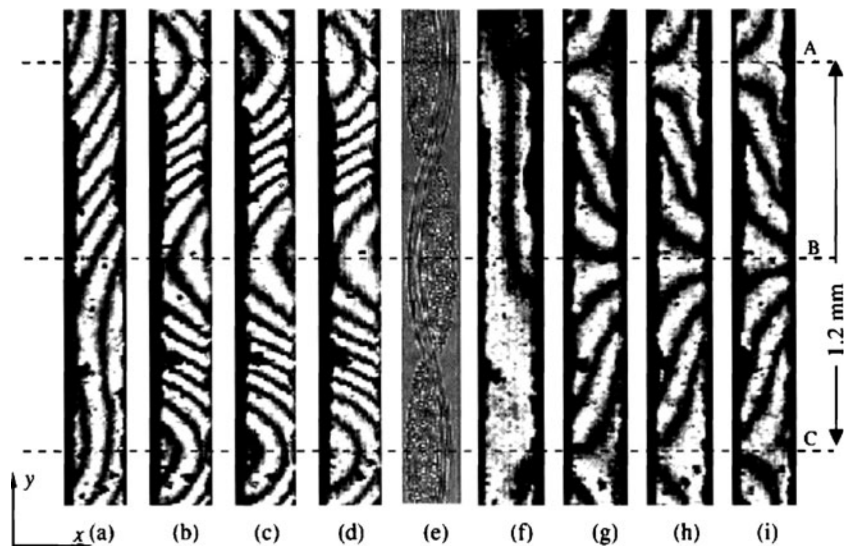

Fig. 19 Moiré fringe patterns in the fill direction at 27°C for (**a**) initial u-field, (**b**) u-field at 0.1 min., (**c**) u-field at 1 min., (**d**) u field at 10 min, (**e**) composite microstructure, (**f**) initial v-field, (**g**) v-field at 0.1 min., (**h**) v-field at 1 min., (**i**) v field at 10 min (Courtesy of Shrotriya)

time (reflecting what was previously measured using strain gages) but the shape and distribution remained almost identical for all the loading cases and sample configurations. Figure 19 represents a sample of the fringe patterns taken on the edge of the composite for various times after the load was applied. In the figure, both the horizontal and vertical displacement fields are presented, as well as a schematic of the fabric architecture.

Damage Initiation

Moiré interferometry was used by Mollenhauer et al. [119] to study damage mechanisms in open-hole tension tests on laminated composites. Figure 20 describes an experimental effort to examine the effects of sub-critical matrix damage (cracks and delaminations) on the strain field in a tensile loaded open-hole composite laminate. In this case, the quasi-isotropic specimen was pre-loaded at several levels to induce various amounts of matrix damage. The figure shows a schematic of the maximum damage extent as well as evidence of the damage influence on the transverse strain component over the whole field of view. After each preload, the specimen was examined in a moiré interferometer at a common, lower load. These strain patterns were then compare, as shown in the line graph. As evident in the graph, a strain concentration in the 0° ply is seen at approximately 1 mm from the hole centerline. This strain concentration is coincident with an underlying 45° matrix crack. The significance of this effect can be seen in the failed specimen image where the failure initiation in the 0° ply can be seen to occur at approximately 1 mm from the hole centerline.

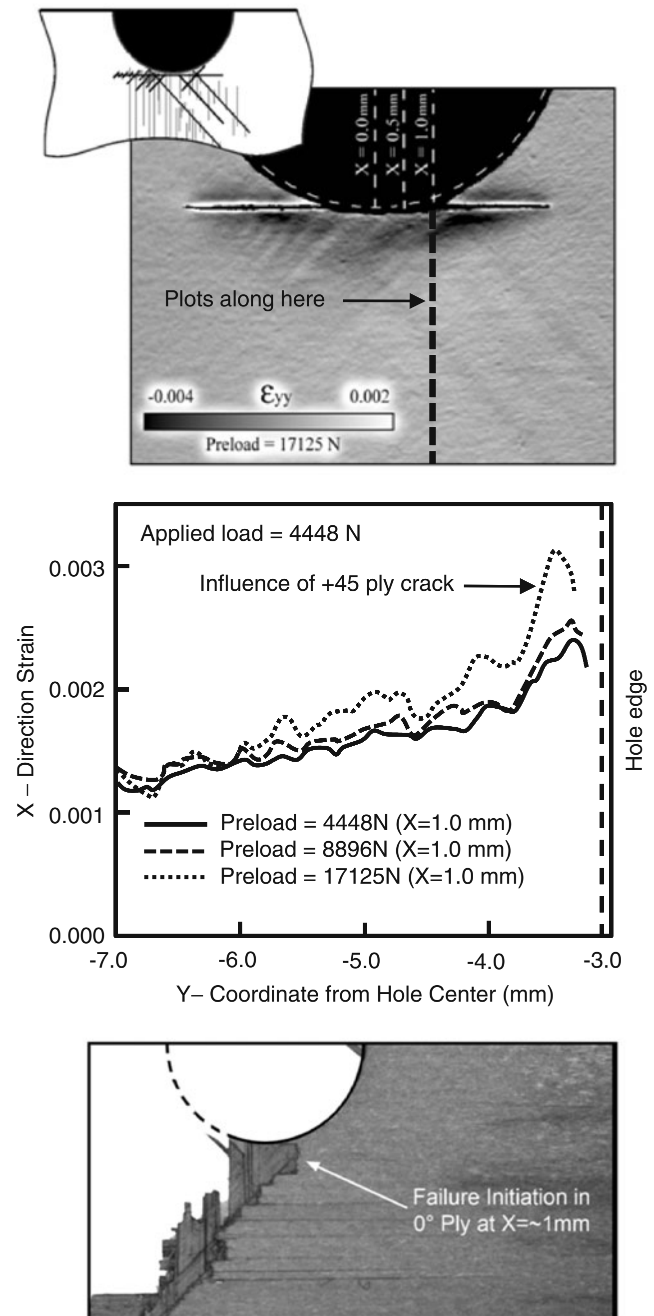

Fig. 20 Evidence of subcritical damage in the form of cracking and delamination can be seen in the strain field acquired via moiré interferometry (Courtesy of D. Mollenhauer)

Fracture Mechanics

Inelastic deformation appears to accompany the fracture process, even for brittle materials. It is recognized as permanent deformation in the neighborhood of the crack path, and for nonmetals it is known as the damage wake. Moiré interferometry has been used extensively for experimental fracture mechanics, most notably, crack tip displacement measurement [120–125] and deformation analyses of fracture zone near a crack tip [126–134].

Nishioka et al. [120] used moiré interferometry to investigate interfacial crack-tip behavior of an epoxy/aluminum bimaterial specimen. Kang and Anderson [121] used a combined Moire-Sagnac interferometry method to measure three-dimensional crack tip deformations at room as well as high temperatures. Kang and Lu [122] investigated the displacement fields near the tip of a crack in a bimaterial joint under mixed-mode loading. Savalia and Tippur [125] mapped the debonding evolution between the inclusion-matrix pair in a composite by recording crack opening displacements using moiré interferometry. The representative surface deformations analyzed in the study are shown in Fig. 21.

Guo and Kobayashi [126] obtained the crack tip displacement fields from moiré interferometry and used the results interactively to drive a finite element (FE) model of double cantilever beam (DCB). Bastawros and Kim [127] utilized moiré interferometry to document the in-plane components

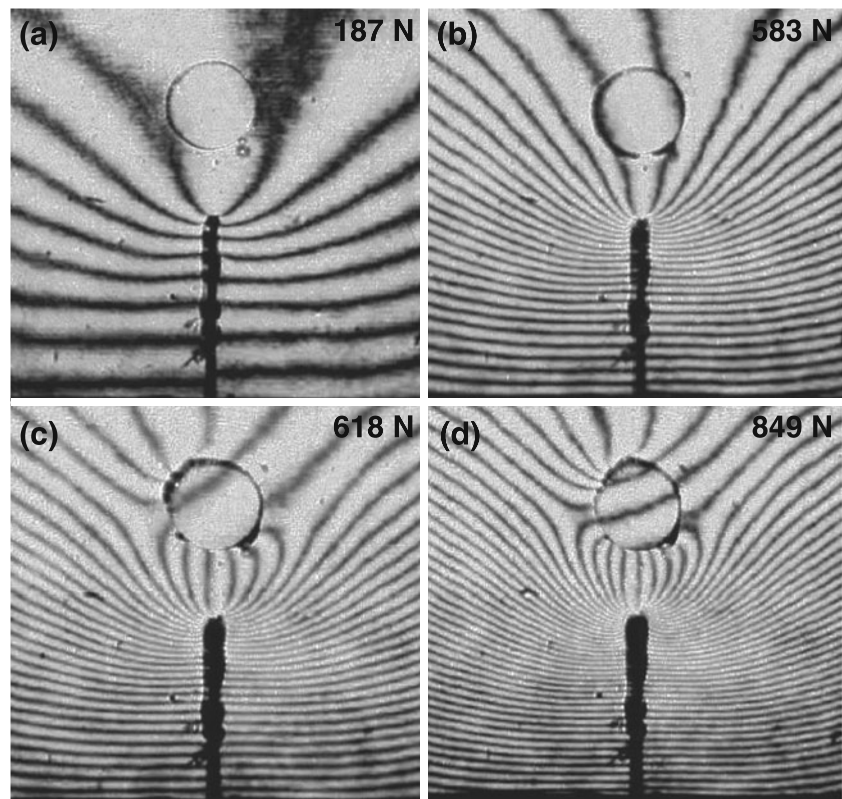

Fig. 21 Selected moiré interferogram of crack-inclusion specimen showing debonding between inclusion and matrix: (**a**), (**b**) Before debonding, (**c**), (**d**) After debonding (Courtesy of H. Tippur, Auburn University)

of the Almansi strain tensor at the microstructural length, near a stationary crack-tip in a four-point-bend specimen of polycrystalline aluminum. Tran and Kobayashi [130] used a hybrid experimental (moiré)-numerical (FEA) procedure to analyze the trailing fracture process zone associated with stable crack growth at room and elevated temperature in high density polycrystalline alumina. The crack bridging stress and the dissipated energy in the fracture process zone were determined at room temperature, 600°C, 800°C, 1,000°C and 1,200°C from moiré fringe patterns (Fig. 22). Ma and Kobayashi [131] and Kojaly et al. [129, 132] used the T-epsilon integral to assess stable crack growth and crack

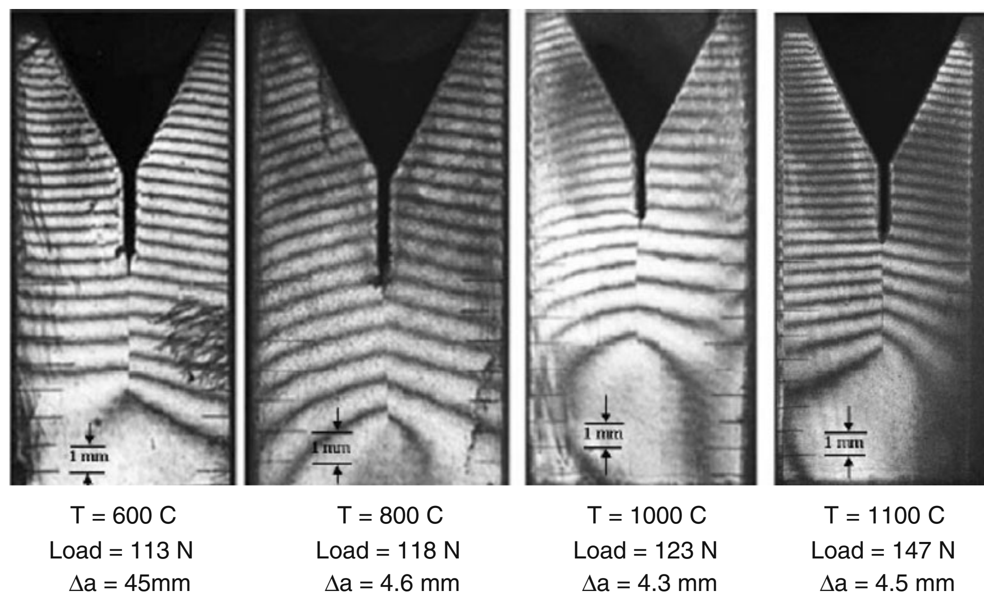

Fig. 22 Moiré interferometry fringe patterns of AL23-1998 WL-DCB specimens (Courtesy of A. Kobayashi, University of Washington)

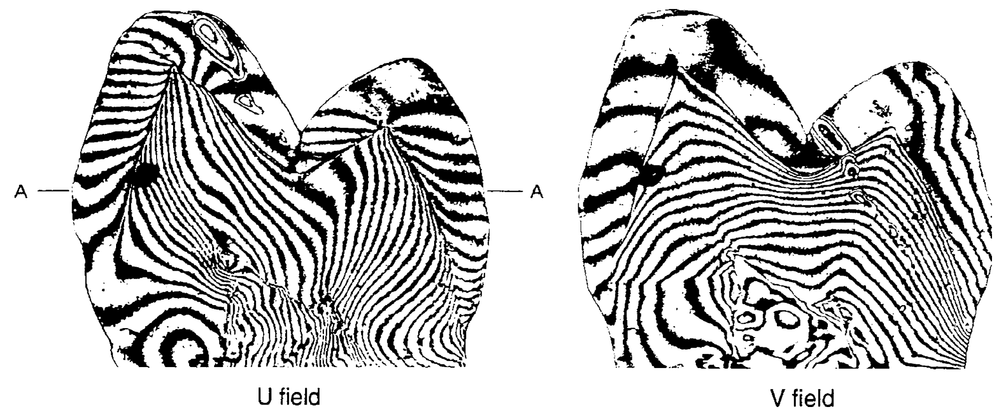

Fig. 23 Differences in moisture state on human teeth can be seen in the moiré fringe patterns (Courtesy of J. Wood, Clemson University)

linkup in 0.8 mm thick 2024-T3 aluminum tension specimens with multiple site damage (MSD) under monotonic and cyclic loads. Liu et al. [133] utilized high temperature moiré interferometry (HTMI), coupled with SEM/EDAX, to analyze the crack growth behavior of Inconel 718. Ramulu et al. [134] utilized moiré interferometry to characterize the fundamental elastic-plastic stress/strain response of friction stir-welded butt joints in thin-sheet, fine grain Ti-6Al-4 V titanium alloy.

The deformation fields around cracks obtained by moiré interferometry have been utilized effectively to determine the stress intensity factor [135–137]. Wang et al. [135] used moiré results to determine the interfacial fracture toughness of a flip-chip package subjected to a constant concentrated line load. McKellar et al. [136] compared complete near-crack-tip fields and singular fields associated with the stress intensity factor, where the use of moiré interferometry to measure crack-tip quantities was discussed. Yoneyama et al. [137] proposed a method for evaluating mode I, mode II and mixed-mode stress intensity factors from in-plane moiré displacement fields. This approach was also used to characterize the coupled electro-elastic fracture behavior of piezo-ceramics [138, 139].

Biomechanics of Teeth

In the human tooth, the structural part is a hard enamel shell surrounding a bone-like material called dentin. When restorations are required to treat decay, breakage, etc., the dentin is exposed and effective adhesion of the restoration material to the dentin is required. Moiré interferometry has been used to determine the deformations of teeth, especially for the mechanics of dentin [87, 140–145].

Wang and Weiner [140] first attempted to map the in-plane strain distribution in slices, from human tooth crowns under compression. It was found that the strain inside enamel was much less than in dentin. Kishen and Asundi [141] investigated the adaptation of dentine to temperature variation using digital moiré interferometry. Arola et al. [142] evaluated the fatigue and fracture properties of bovine dentin using the in-plane displacement fields during stable crack growth.

Wood et al. [143] evaluated the effects of changes in humidity on the dimensional changes in dentin disks constrained by enamel and in unconstrained dentin. The moiré fringe patterns in Fig. 23 represent the change in deformation between the moisture states. The results indicated that there were wide variations in strain between the two specimen geometries. Later Kishen and Asundi [145] used a similar approach to investigate the role of free water on the in-plane, mechanical strain response in dentine structure.

Conclusion

The experimental technique of moiré interferometry is a mature technology and has been utilized in wide variety of applications in solid mechanics and materials. Over the past decade, most of the applications have been in the areas of microelectronics, material characterization, micromechanics, residual stress, composites, facture mechanics and biomechanics. With its high spatial and measurement resolution, it is expected that moiré interferometry will continue to play an important role in the understanding of mechanical phenomena for years to come.

References

1. Post D, Han B, Ifju PG (1994) High sensitivity moiré: experimental analysis for mechanics and materials. Mechanical Engineering Series, Springer-Verlag
2. Knauss WG (2000) Perspectives in experimental solid mechanics. Int J Solids Struct 37(1–2):251–266
3. Post D (1991) Moiré interferometry—advances and applications. Exp Mech 31(3):276–280
4. Post D (1982) Developments in moiré interferometry. Opt Eng 21(3):458–467

5. Post D, Han B (2008) Moiré interferometry. Handbook of experimental solid mechanics. Springer Science and Business Media, LLC, New York, pp 627–653
6. Perry KE, McKelvie J (1993) A comparison of phase-shifting and Fourier methods in the analysis of discontinuous fringe patterns. Opt Lasers Eng 19(4–5):269–284
7. McKelvie J (1998) Moiré strain analysis: an introduction, review and critique, including related techniques and future potential. J Strain Anal Eng Des 33(2):137–151
8. McKelvie J (1997) Thermal-insensitive moiré interferometry. Opt Lett 22(1):55–57
9. McKelvie J (1990) On moiré interferometry and the level of detail that it may reveal legitimately. Opt Lasers Eng 12(2–3):81–99
10. Walker CA (1994) A historical review of moiré interferometry. Exp Mech 34(4):281–299
11. Walker CA (1988) A review of moire interferometry. Opt Lasers Eng 8:213–262
12. Walker CA (1988) Moiré interferometry for strain analysis. Opt Lasers Eng 8:1–50
13. Cloud G (1994) Optical methods of engineering analysis. Cambridge University Press, UK
14. Dai FL, McKelvie J, Post D (1990) An interpretation of moiré interferometry from wavefront interference theory. Opt Lasers Eng 12(2–3):101–118
15. Fang J, Dai FL (1990) A new real-time method of moiré interferometry for displacement derivative fringe patterns. Opt Lasers Eng 13(1):51–58
16. Qing XL, Qin YW, Dai FL (1995) Optical fringe multiplication in moiré interferometry. Appl Opt 34(31):7291–7294
17. Qing XL, Qin YW, Dai FL (1996) Experimental investigation of micromechanical behavior of advanced materials by moiré interferometry. Opt Lasers Eng 25(2–3):179–189
18. Morimoto Y, Hayashi T, Wada K (1989) High-sensitivity measurement of strain by moiré interferometry. JSME Int J Ser I Solid Mech Strength Mater 32(1):122–127
19. Morimoto Y, Gascoigne HE, Post D (1994) Carrier pattern-analysis of moiré interferometry using the Fourier-transform moiré method. Opt Eng 33(8):2646–2653
20. Guo Y, Lim CK, Chen WT, Woychik CG (1993) Solder ball connect (sbc) assemblies under thermal loading.1. Deformation measurement via moire interferometry, and its interpretation. IBM J Res Dev 37(5):635–647
21. Han B, Guo Y (1995) Thermal deformation analysis of various electronic packaging products by moire and microscopic moire interferometry. J Electron Packag 117(3):185–191
22. Post D, Wood J (1989) Determination of thermal strains by moiré interferometry. Exp Mech 29(3):318–322
23. Wu TY, Guo Y, Chen WT (1993) Thermal-mechanical strain characterization for printed wiring boards. IBM J Res Dev 37 (5):621–634
24. Han B, Chopra M, Park S, Li L, Verma K (1996) Effect of substrate CTE on solder ball reliability of flip-chip PBGA package assembly. J Surf Mount Technol 9:43–52
25. Han B, Guo Y (1996) Determination of an effective coefficient of thermal expansion of electronic packaging components: a whole-field approach. IEEE Trans Compon Packag Manuf Technol A: 19(2):240–247
26. Han B, Guo Y, Lim CK, Caletka D (1996) Verification of numerical models used in microelectronics packaging design by interferometric displacement measurement methods. J Electron Packag 118(3):157–163
27. Han B (1997) Deformation mechanism of two-phase solder column interconnections under highly accelerated thermal cycling condition: an experimental study. J Electron Packag 119(3):189–196
28. Han B (1998) Recent advancements of moire and microscopic moire interferometry for thermal deformation analyses of microelectronics devices. Exp Mech 38(4):278–288
29. Deshpande AM, Subbarayan G, Rose D (2000) A system for first order reliability estimation of solder joints in area array packages. J Electron Packag 122(1):6–12
30. Han B, Kunthong P (2000) Micro-mechanical deformation analysis of surface laminar circuit in organic flip-chip package: an experimental study. J Electron Packag 122(4):294–300
31. Mercado LL, Sarihan V, Guo YF, Mawer A (2000) Impact of solder pad size on solder joint reliability in flip chip PBGA packages. IEEE Trans Adv Packag 23(3):415–420
32. Yim MJ, Jeon YD, Paik KW (2000) Reduced thermal strain in flip chip assembly on organic substrate using low CTE anisotropic conductive film. IEEE Trans Electron Packag Manuf 23(3):171–176
33. Han B, Post D, Ifju P (2001) Moiré interferometry for engineering mechanics: current practice and future development. J Strain Anal 36(1):101–117
34. Han B, Wu Z, Cho S (2001) Measurement of thermal expansion coefficient of flexible substrate by moire interferometry. Exp Tech 25(3):22–25
35. Han B (2003) Thermal stresses in microelectronics subassemblies: quantitative characterization using photomechanics methods. J Therm Stresses 26:583–613
36. Ratanawilai TB, Hunter B, Subbarayan G, Rose D (2003) A study on the variation of effective CTE of printed circuit boards through a validated comparison between strain gages and Moire interferometry. IEEE Trans Compon Packag Technol 26(4):712–718
37. Chaparala S, Pitarresi JM, Parupalli S, Mandepudi S, Meilunas M (2006) Experimental and numerical investigation of the reliability of double-sided area array assemblies. J Electron Packag 128(4):441–448
38. Kwon WS, Yang SY, Lee SB, Paik KW (2006) Contraction stresses development of anisotropic conductive films (ACFs) flip chip interconnection: Prediction and measurement. IEEE Trans Compon Packag Technol 29(3):688–695
39. Morita Y, Arakawa K, Todo M, Kaneto M (2006) Experimental study on the thermo-mechanical effects of underfill and low-CTE substrate in a flip-chip device. Microelectron Reliab 46(5–6):923–929
40. Tsai MY, Chiang WC, Liu TM, Hsu GH (2006) Thermal deformation measurements and predictions of MAP-BGA electronic packages. Microelectron Reliab 46(2–4):476–486
41. Han B (2007) 14. Characterization of stresses and strains in microelectronic and photonic devices using photomechanics methods. In: Suhir YCLAA (ed) Micro-and optoelectronic materials and structures: Physics, mechanics, design, reliability, and packaging. Springer, New York
42. Basaran C, Cartwright A, Zhao Y (2001) Experimental damage mechanics of microelectronics solder joints under concurrent vibration and thermal loading. Int J Damage Mech 10(2):153–170
43. Liu H, Basaran C, Cartwright AN, Casey W (2004) Application of moire interferometry to determine strain fields and debonding of solder joints in BGA packages. IEEE Trans Compon Packag Technol 27(1):217–223
44. Tunga K, Sitararnan SK (2007) An expedient experimental technique for the determination of thermal cycling fatigue life for BGA package solder balls. J Electron Packag 129(4):427–433
45. Kwon WS, Yim MJ, Paik KW, Ham SJ, Lee SB (2005) Thermal cycling reliability and delamination of anisotropic conductive adhesives flip chip on organic substrates with emphasis on the thermal deformation. J Electron Packag 127(2):86–90

46. Zhao Y, Basaran C, Cartwright A, Dishongh T (2000) Thermomechanical behavior of micron scale solder joints under dynamic loads. Mech Mater 32(3):161–173
47. Stout EA, Sottos NR, Skipor AF (2000) Mechanical characterization of plastic ball grid array package flexure using Moire interferometry. IEEE Trans Adv Packag 23(4):637–645
48. Wang GT, Merrill C, Zhao JH, Groothuis SK, Ho PS (2003) Packaging effects on reliability of Cu/Low-k interconnects. IEEE Trans Device Mater Reliab 3(4):119–128
49. Joo J, Cho S, Han B (2005) Characterization of flexural and thermomechanical behavior of plastic ball grid package assembly using moire interferometry. Microelectron Reliab 45(3–4):637–646
50. Cho S, Han B (2002) Observing real-time thermal deformations in electronic packaging. Exp Tech 26(3):25–29
51. Cho SM, Han BT, Joo J (2004) Temperature dependent deformation analysis of ceramic ball grid array package assembly under accelerated thermal cycling condition. J Electron Packag 126(1):41–47
52. Han L, Voloshin A, Emri I (2004) Study of the multilayer PCBCTEs by moire interferometry. Opt Lasers Eng 42(6):613–626
53. Joo J, Cho S (2004) Evaluation of thermal deformation model for BGA packages using moire interferometry. Ksme Int J 18 (2):230–239
54. Shi XQ, Pang HLJ, Zhang XR (2004) Investigation of long-term reliability and failure mechanism of solder interconnections with multifunctional micro-moire interferometry system. Microelectron Reliab 44(5):841–852
55. Zhong ZW, Wong KW, Shi XQ (2004) Interfacial behavior of a flip-chip structure under thermal testing. IEEE Trans Electron Packag Manuf 27(1):43–48
56. Kwon WS, Ham SJ, Paik KW (2006) Deformation mechanism and its effect on electrical conductivity of ACF flip chip package under thermal cycling condition: an experimental study. Microelectron Reliab 46(2–4):589–599
57. Yang SY, Jeon YD, Lee SB, Paik KW (2006) Solder reflow process induced residual warpage measurement and its influence on reliability of flip-chip electronic packages. Microelectron Reliab 46(2–4):512–522
58. Yang SY, Lee WJ, Jeong SH, Lee SJ (2006) Structural reliability assessment of multi-stack package (MSP) under high temperature storage (HTS) testing condition, Microelectron Reliab 46(9–11):1904–1909
59. Zhang YL, Shi DXQ, Zhou W (2006) Reliability study of underfill/chip interface under accelerated temperature cycling (ATC) loading. Microelectron Reliab 46(2–4):409–420
60. Zhong ZW, Wong KW, Shi XQ (2006) Deformations of a simplified flip chip structure under thermal testing inspected using a real-time Moire technique. Int J Adv Manuf Technol 27 (7–8):708–714
61. Joo JW, Choa SH (2007) Deformation behavior of MEMS gyroscope sensor package subjected to temperature change. IEEE Trans Compon Packag Technol 30(2):346–354
62. Morita Y, Arakawa K, Todo M (2007) High-sensitivity measurement of thermal deformation in a stacked multichip package. IEEE Trans Compon Packag Technol 30(1):137–143
63. Tunga KR, Sitaraman SK (2008) Using carrier fringes to study the high deformation behavior of a BGA package dwell times. Exp Mech 48(3):355–365
64. Zhang Y, Liu J, Larsson R, Watanabe I (2008) Experimental investigation and micropolar modelling of the anisotropic conductive adhesive flip-chip interconnection. J Adhes Sci Technol 22(14):1717–1731
65. Zhang Y, Liu JH, Larsson R (2008) Experimental and modeling of the stress-strain behavior of a BGA interconnect due to thermal load. J Electron Packag 130(2). Jun
66. Park SB, Joshi R, Ahmed I, Chung SW (2008) Comparative studies on solder joint reliability of plastic and ceramic ball grid array packages of the same form factor under power and accelerated thermal cycling. J Electron Packag 130(4). Dec
67. Yang SY, Kim I, Lee SB (2008) A study on the thermal fatigue behavior of solder joints under power cycling conditions. IEEE Trans Compon Packag Technol 31(1):3–12
68. Ye H, Hopkins DC, Basaran C (2003) Measurement of high electrical current density effects in solder joints. Microelectron Reliab 43(12):2021–2029
69. Ye H, Basaran C, Hopkins DC (2004) Deformation of solder joint under current stressing and numerical simulation-I. Int J Solids Struct 41(18–19):4939–4958
70. Stellrecht E, Han B, Pecht M (2003) Measurement of the hygroscopic swelling coefficient in mold compounds using moire interferometry. Exp Tech 27(4):40–44
71. Stellrecht E, Han BT, Pecht MG (2004) Characterization of hygroscopic swelling behavior of mold compounds and plastic packages. IEEE Trans Compon Packag Technol 27(3):499–506
72. Tsai MY, Huang CH, Huang CY (2006) Hygrothermal effect on deformations of QFN electronic packaging, J Mech 22(4):271–279
73. Park JH, Jang KW, Paik KW, Lee SB (2010) A study of hygrothermal behavior of ACF flip chip packages with Moire interferometry. IEEE Trans Compon Packag Technol 33(1):215–221
74. Perry KE, Labossiere PE, Steffler E (2007) Measurement of deformation and strain in Nitinol. Exp Mech 47:372–380
75. Guo Z, Xie H, Liu B, Dai F, Chen P, Zhang Q, Huang F (2006) Study on deformation of polycrystalline aluminum alloy using moiré interferometry. Exp Mech 46:699–711
76. Wang Z, Cardenas-Garcia JF, Han B (2005) Inverse method to determine elastic constants using a circular disk and moiré interferometry. Exp Mech 45(1). Feb
77. Molimard J, Le Riche R, Vautrin A, Lee JR (2005) Identification of the four orthotropic plate stiffnesses using a single open-hole tensile. Test J Exp Mech 45:404–441
78. Chen TC, Ferraro CC, Yin WQ, Ishee CA, Ifju PG (2010) A novel two-dimensional method to measure surface shrinkage in cementitious materials. Cem Concr Res 40(5):687–698
79. Shield TW, Kim K-S (1991) Diffraction theory of optical interference moiré and a device for production of variable virtual reference gratings: a moiré microscope. Exp Mech 31(2)
80. Han B (1992) Higher sensitivity moiré interferometry for micromechanics studies. Opt Eng 31(7):1517–1526
81. Liou NS, Prakash V (2000) A moire microscope for finite deformation micro-mechanical studies. Exp Mech 40(4):351–360
82. Han B, Post D (1992) Immersion interferometer for microscopic moiré interferometry. Exp Mech 32(1):38–41
83. La Porta FA, Huntley JM, Chung TE, Faulkner RG (2000) High-magnification moire interferometer for crack tip analysis of steels. Exp Mech 40(1):90–95
84. Bastawros AF, Kim KS (2000) Experimental analysis of near-crack-tip plastic flow and deformation characteristics (I): polycrystalline aluminum. J Mech Phys Solids 48(1):67–98
85. Han B (1996) Micromechanical deformation analysis of b alloy Titanium in elastic and elastic/plastic tension. Exp Mech 36 (2):120–126
86. Han B (1996) Micromechanical thermal deformation analysis of unidirectional Boron/Aluminum metal-matrix composite. Opt Lasers Eng 24:455–466
87. Wood JD, Sobolewski P, Thakur V, Arola D, Nazari A, Tay FR, Pashley DH (2008) Measurement of microstrains across loaded resin-dentin interfaces using microscopic moire interferometry. Dent Mater 24(7):859–866

88. Mathar J (1934) Determination of initial stresses by measuring the deformation around drilled holes. Trans of ASME 56(4):249–254
89. Soete W, Vancrombrugge R (1950) An industrial method for the determination of residual stresses. Proc SESA 8(1):17–28
90. Rendler NJ, Vigness I (1966) Hole-drilling strain-gage method of measuring residual stresses. Exp Mech 6(12):577–586
91. Gadd CW (1946) Residual stress indications in brittle lacquer. Proc SESA 4:74–77
92. Zandman F (1960) Photoelastic-coating technique for determining stress distribution in welded structures. Weld J 39(5):191s–198s
93. Nelson DV, McCrickerd J (1986) Residual stress determination through combined use of holographic interferometry and blind-hole drilling. Exp Mech 26(4):371–378
94. Hung YY, Long KW, Wang JQ (1997) Measurement of residual stress by phase shifting shearography. Opt Lasers Eng 27:61–73
95. Li K (1997) Application of interferometric strain rosette to residual stress measurements. Opt Lasers Eng 27:125–136
96. McGinnis MJ, Pessiki S, Turner H (2005) Application of three-dimensional digital image correlation to the core-drilling method. Exp Mech 45(4):359–367
97. Schajer GS (2010) Advances in hole-drilling residual stress measurement. Exp Mech 50:159–168
98. Nelson DV (2010) Residual stress determination by hole drilling combined with optical methods. Exp Mech 50:145–158
99. Nicoletto G (1991) Moiré interferometry determination of residual stresses in the presence of gradients. Exp Mech 31(3)
100. Chen J, Peng Y, Zhao S (2009) Hole-drilling method using grating rosette and moire interferometry. Acta Mech Sin 25:389–394
101. Ya M, Miao H, Zhang X, Lu J (2006) Determination of residual stress by use of phase shifting moiré interferometry and hole-drilling method. Opt Lasers Eng 44(1):68–79
102. Ya M, Dai F, Xie H, Lu J (2003) Measurement of non-uniform residual stresses by combined moiré interferometry and hole-drilling method: theory, experimental method and applications. Acta Mech Sin 19(9). December
103. Ya M, Xing Y, Dai F, Lu K, Lu J (2003) Study of residual stress in surface nanostructured aisi 316 l stainless steel using two mechanical methods. Surf Coat Technol 68(2–3):148–155
104. Wu Z, Lu J, Han B (1998) Study of residual stress distribution by a combined method of moiré interferometry and incremental hole-drilling, part i: theory. J Appl Mech 65:837–843
105. Wu Z, Lu J, Han B (1998) Study of residual stress distribution by a combined method of moiré interferometry and incremental hole-drilling, part ii: implementation. J Appl Mech 65:844–850
106. Wu Z, Niu X, Lu J, and Ifju P (1998) Study of process-induced residual stress in orthotropic composite laminate—carbon/epoxy [02/902]2s. SEM Spring Conference.
107. Shankar K, Xie H, Wei R, Asundi A, Boay CG (2004) A study on residual stress in polymer composites using moire interferometry. Adv Compos Mater 13(3–4):237–253
108. Joh D, Byun KY, Ha J (1993) Thermal residual stresses in thick graphite/epoxy composite laminates-uniaxial approach. Exp Mech 33(1)
109. Gascoigne HE (1994) Residual surface stresses in laminated cross-ply fiber-epoxy composite materials. Exp Mech 34(1):27–36
110. Bowman CKB, Mollenhauer DH (2002) Experimental investigation of residual stresses in layered materials using moiré interferometry. J Electron Packag 124(4):340–344
111. Lee DJ, Czarnek R (1991) Measuring residual strains in composite panels using moiré interferometry. SEM Spring Conference on Experimental Mechanics, Milwaukee, WI, Proceedings (A93-16601 04-39), June 10–13, pp 405–415
112. Schoeppner GA, Mollenhauer DH, Iarve EV (2004) Prediction and measurement of residual strains for composite bonded joint. Mech Comp Mater 40(2)
113. Ifju PG, Kilday BC, Niu X, Liu SC (1999) A novel means to determine residual stress in laminated composites. J Compos Mater 33(16)
114. Ifju PG, Niu X, Kilday BC, Liu S-C, Ettinger SM (2000) Residual strain measurement in composites using the cure-referencing method. J Exp Mech 40(1):22–30
115. Burr S, Ifju PG, Morris D (1995) Optimizing strain gage size for textile composites. Exp Tech 19(5):25–27
116. Ifju PG, Masters JE, Jackson WC (1995) Using moiré interferometry to aid in standard test method development for textile composite materials. J Comp Sc and Tech 53:155–163
117. Lee JR, Molimard J, Vautrin A, Surrel Y (2004) Application of grating shearography and speckle pattern shearography to mechanical analysis of composite, composite part a. Appl Sci Manuf 35:965–976
118. Shrotriya P, Sottos NR (2004) Local time-temperature-dependent deformation of a woven composite. J Exp Mech 44(4)
119. Mollenhauer D, Iarve EV, Kim R, Langley B (2006) Examination of ply cracking in composite laminates with open holes: a moiré interferometry and numerical study. Appl Sci Manuf 37 (2):282–294
120. Nishioka T, Yao JL, Sakakura K, Epstein JS (2000) Measurements of near-tip displacement fields, separated J integrals and separated energy release rates for interfacial cracks using phase-shifting Moire interferometry. Jsme Int J Ser A Solid Mech Mater Eng 43(4):334–342
121. Kang BSJ, Anderson SM (2001) Three-dimensional crack tip deformation measurement using combined Moire-Sagnac interferometry. Exp Mech 41(1):84–91
122. Kang YL, Lu H (2002) Investigation of near-tip displacement fields of a crack normal to and terminating at a bimaterial interface under mixed-mode loading. Eng Fract Mech 69(18):2199–2208
123. Dai FL, Shang HX, Fang DN, Wang GT, Jiang XL (2004) Experimental study on fracture mechanism of aluminum plates in tension and laser irradiation with high temperature moire interferometry. In: Kishimoto K, Kikuchi M, Shoji T et al. (eds) Advances in fracture and failure prevention, Pts 1 and 2, Key Engineering Materials. Trans Tech Publications Ltd, Zurich-Uetikon, pp 213–218
124. MacKenzie PM (2007) Moire interferometry applied to fracture in titanium tubes. Proc Inst Mech Eng, L: J Mater Des Appl 221 (L3):131–141
125. Savalia PC, Tippur HV (2007) A study of crack-inclusion interactions and matrix-inclusion debonding using Moire interferometry and finite element method. Exp Mech 47(4):533–547
126. Guo ZK, Kobayashi AS, Hay JC, White KW (1999) Fracture process zone modeling of monolithic Al2O3. Eng Fract Mech 63 (2):115–129
127. Bastawros AF, Kim KS (2000) Experimental analysis of near-crack-tip plastic flow and deformation characteristics (I): polycrystalline aluminum. J Mech Phys Solids 48(1):67–98
128. Todo M, Arakawa K, Takahashi K (2000) Nonlinear displacement field in the vicinity of notch-tip in rubber toughened PMMA. In: Hwang W, Han KS (eds) Fracture and strength of solids, Pts 1 and 2, Key Engineering Materials. Trans Tech Publications Ltd, Zurich-Uetikon, pp 409–414
129. Kokaly MT, Lee J, Kobayashi AS (2001) Dynamic ductile fracture of 7075-T6—an experimental analysis. Int J Solids Struct 38(10–13):1935–1942

130. Tran DK, Kobayashi AS, White KW (2001) Crack growth in alumina at high temperature. Eng Fract Mech 68(2):149–161
131. Ma L, Kobayashi AS, Atluri SN, Tan PW (2002) Crack linkup: an experimental analysis. Exp Mech 42(2):147–152
132. Kokaly MT, Lee J, Kobayashi AS (2003) Moire interferometry for dynamic fracture study. Opt Lasers Eng 40(4):231–247
133. Liu XB, Kang B, Carpenter W, Barbero E (2004) Investigation of the crack growth behavior of Inconel 718 by high temperature Moire interferometry. J Mater Sci 39(6):1967–1973
134. Ramulu M, Labossiere P, Greenwell T (2010) Elastic-plastic stress/strain response of friction stir-welded titanium butt joints using moire interferometry. Opt Lasers Eng 48(3):385–392
135. Wang JJ, Zou DQ, Lu MF, Ren W, Liu S (1999) Evaluation of interfacial fracture toughness of a flip-chip package and a bimaterial system by a combined experimental and numerical method. Eng Fract Mech 64(6):781–797
136. McKellar DK, Hills DA, Nowell D (2000) A comparison between actual and stress intensity near-crack-tip elastic fields. Int J Fatigue 22(7):551–558
137. Yoneyama S, Ogawa T, Kobayashi Y (2007) Evaluating mixed-mode stress intensity factors from full-field displacement fields obtained by optical methods. Eng Fract Mech 74 (9):1399–1412
138. Fang DN, Liu ZW, Xie HM, Li S, Dai FL, Bing QD (2004) Study on fracture behavior of ferroelectric ceramics under combined electromechanical loading by using a moire interferometry technique. Acta Mech Sin 20(3):263–269
139. Chen MC, Ping XC, Xie HM, Liu ZW (2008) Numerical and experimental analyses of singular electro-elastic fields around a V-shaped notch tip in piezoelectric materials. Eng Fract Mech 75 (18):5029–5041
140. Wang RZ, Weiner S (1998) Strain-structure relations in human teeth using Moire fringes. J Biomech 31(2):135–141
141. Kishen A, Asundi A (2001) Investigations of thermal property gradients in the human dentine. J Biomed Mater Res 55(1):121–130
142. Arola D, Rouland JA, Zhang D (2002) Fatigue and fracture of bovine dentin. Exp Mech 42(4):380–388
143. Wood JD, Wang RZ, Weiner S, Pashley DH (2003) Mapping of tooth deformation caused by moisture change using moire interferometry. Dent Mater 19(3):159–166
144. Kishen A, Asundi A (2005) Photomechanical investigations on the stress-strain relationship in dentine macrostructure. J Biomed Opt 10(3). May–Jun
145. Kishen A, Asundi A (2005) Experimental investigation on the role of water in the mechanical behavior of structural dentine. J Biomed Mater Res A 73A(2):192–200